Contribution from the Department of Chemistry, Northwestern University, Evanston, Illinois 60201

Spectroscopic and Theoretical Studies of Iron Tricarbonyl 1,4-Dimethyltetraazadiene and Related Complexes. Evidence for a Hückel Aromatic Metal–Nitrogen Ring

WILLIAM C. TROGLER,* CURTIS E. JOHNSON, and DONALD E. ELLIS

Received August 11, 1980

Complexes of the type $Fe(CO)_3(N_4(R)_2)$, $Fe(CO)_2L(N_4(CH_3)_2)$, $Fe(CO)L_2(N_4(CH_3)_2)$, and $Fe(P(OCH_3)_3)_3(N_4(CH_3)_2)$ [L = $P(C_6H_5)_3$, $P(CH_3)_3$, $P(OCH_3)_3$; R = CH_3, C_6H_5] exhibit two intense electronic transitions at 470–520 and 349–390 nm. These are attributed to the presence of a low-lying unoccupied metallocycle π^* orbital. The d^8 $Fe(CO)_3$ fragment possessing two d_π electrons can interact with the four p_π electrons of the N_4R_2 ligand to create a six π-electron (Hückel aromatic) cyclic system. Both Hückel MO and SCC–DV–Xα calculations support the qualitative picture, and the latter study provides a quantitative account of the optical spectroscopic data. The vapor-phase He I photoelectron spectrum of $Fe(CO)_3(N_4(CH_3)_2)$ has been measured. Ionizations in the 8–11-eV spectral region arise from orbitals containing dominant metal d character, in addition to N_4R_2 lone-pair and p_π character. Orbital density plots for the five FeN_4 π orbitals are discussed. The theoretical data suggest that the N_4R_2 ligand rivals carbon monoxide as a π-acceptor ligand, and vapor-phase IR spectra support this conclusion.

Introduction

Unsaturated metallocycles offer the possibility of π delocalization, owing to the presence of partly occupied π orbitals on both the metal and ligand. Thorn and Hoffmann[1] recently examined complexes which contain the metallocyclopentadiene moiety (I). From the X-ray structural data and with the aid

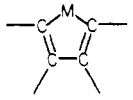

I

of Extended Hückel molecular orbital calculations, they concluded that delocalization of the metallocycle π-electron system was slight. We have been examining the ground- and excited-state chemistry of metallotetraazadiene complexes (II),

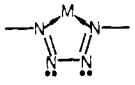

II

and some possible bonding modes for this nitrogen-based ring system are depicted in Figure 1.

The first metal tetraazadiene complex, $Fe(CO)_3(N_4(CH_3)_2)$, was discovered[2] in 1967 and found to adopt a planar FeN_4 configuration.[3] Interesting structural aspects were the short (1.85 Å) Fe–N bonds and the equivalent N–N bond lengths (1.32 Å). A diene resonance structure **1** (see Figure 1) was favored by Doedens;[3] however, the standard deviations for the N–N bond lengths were large (±0.07 Å). Preliminary structural studies of Einstein and Sutton[4] for the complex $[Ir(N_4(C_6H_4F)_2)(CO)(PPh_3)_2]BF_4$ supported resonance form **2** (Figure 1). Again the N_4 ring was planar; however, the metal was displaced 0.12 Å out of plane. On the basis of further refinements,[5] a tetrazene type of resonance form **3** (Figure 1) was suggested. Resonance structures **1**–**3** differ substantially in that the N_4R_2 ligand acts as a 4- or 2-electron donor in **1** or **2**, respectively, and as a 2-electron σ donor and 2-electron π donor in **3**. These differing formulations are surprising since the iron(0) and iridium(I) complexes are isoelectronic. A contributing resonance form which had not been discussed is **4** (Figure 1). The apparent Fe–N multiple bonding, equivalent N–N bond lengths, and planarity of the Doedens structure might argue for its importance, although it violates the 18-electron rule. Resonance structure **5** and its partner may also contribute to nonplanar systems[5] and have the advantage of preserving the 18-electron rule.

More recently an X-ray structure analysis of a bis(tetraazadiene) complex of nickel[6] exhibited nearly equivalent N–N bond lengths of 1.325 (3) and 1.319 (4) Å in the N_4 ligand. The authors attributed this to a resonance hybrid of structures **1** and **2**. Suitable crystals of the isoelectronic complex $(\eta^5\text{-}C_5H_5)Co(N_4(C_6F_5)_2)$ have also been obtained, and an X-ray structure analysis has been performed[7] at −150 °C. Observed Co–N bonds are quite short (1.802 (2) and 1.819 (2) Å), and there are two long (1.360 (2) and 1.355 (2) Å) and one short (1.279 (2) Å) N–N distances in the planar CoN_4 ring. This data supports the importance of resonance form **4** in addition to possibly **5** and its partner; however, no simple valence-bond representation can account for all the known structures. This ambiguity should be resolved by a molecular orbital model. Furthermore, it would be desirable to explain the apparent differences between the carbon- and nitrogen-based metallocycles. Electronic structural aspects of the $Fe(CO)_3$ moiety are well understood,[8] and we therefore chose to focus on $Fe(CO)_3(N_4(CH_3)_2)$ and its derivatives.

Experimental Section

Spectra. Details of the matrix isolation apparatus[9] and the photoionization spectrometer[10] have been published. Iron tricarbonyl 1,4-dimethyltetraazadiene sublimes readily at 25 °C, and it was possible to prepare matrices by the pulsed method.[11] The room-temperature vapor pressure was also sufficient to obtain reasonable photoelectron spectra with only 1 h of data acquisition time. Gas-phase IR spectra were recorded on a Nicolet 7199 FT IR. For these measurements a home-built 10-cm gas cell (NaCl windows) was employed, and the instrumental resolution was 0.01 cm^{-1}. Solution UV–vis spectra were recorded with a Perkin-Elmer 320 spectrophotometer. Spectral solvents were distilled under nitrogen from an

(1) Thorn, D. L.; Hoffmann, R. *Nouv. J. Chim.* **1979**, *3*, 39–45.
(2) Dekker, M.; Knox, G. R. *Chem. Commun.* **1967**, 1243, 1244.
(3) Doedens, R. J. *Chem. Commun.* **1968**, 1271, 1272.
(4) Gilchrist, A. B.; Einstein, F. W. B.; Rayner-Canham, G. W.; Sutton, D. *J. Am. Chem. Soc.* **1971**, *83*, 1826, 1827.
(5) Einstein, F. W. B.; Sutton, D. *Inorg. Chem.* **1972**, *11*, 2827–2831. Gilchrist, A. B.; Sutton, D. *Can. J. Chem.* **1974**, *52*, 3387–3393.
(6) Overbosch, P.; van Koten, G.; Overbeek, O. *J. Am. Chem. Soc.* **1980**, *102*, 2091–2093.
(7) Gross, M. E.; Trogler, W. C.; Ibers, J. A. *J. Am. Chem. Soc.* **1981**, *103*, 192, 193.
(8) Elian, M.; Hoffmann, R. *Inorg. Chem.* **1975**, *14*, 1058–1076. Elian, M.; Chen, M. L.; Mingos, D. M. P.; Hoffmann, R. *Inorg. Chem.* **1976**, *15*, 1148–1155.
(9) Trogler, W. C.; Desjardins, S. R.; Solomon, E. I. *Inorg. Chem.* **1979**, *18*, 2131–2136.
(10) Berkowitz, J. *J. Chem. Phys.* **1972**, *56*, 2766–2774. Trogler, W. C.; Ellis, D. E.; Berkowitz, J. *J. Am. Chem. Soc.* **1979**, *101*, 5896–5901.
(11) Rochkind, M. M. *Spectrochim. Acta, Part A* **1971**, *27A*, 547–568. Perutz, R. N.; Turner, J. J. *J. Chem. Soc., Faraday Trans. 2* **1973**, *69*, 452–461.

0020-1669/81/1320-0980$01.25/0

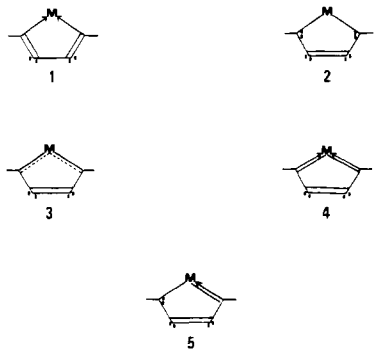

Figure 1. Some possible resonance structures for metal–"tetraazadiene" complexes.

appropriate drying agent prior to use.

Synthesis. $Fe(CO)_3(N_4(R)_2)$ complexes were prepared by the reaction of $Fe_2(CO)_9$ with the appropriate organic azide in diethyl ether at room temperature.[12] *Caution: organic azides are high explosives!* Ligand-substituted derivatives of $Fe(CO)_xL_y(N_4(CH_3)_2)$ (x = 0, 1, 2; y = 3, 2, 1) were prepared thermally (y = 1) or photochemically (y = 2, 3). Full details of the synthesis will be published in a paper on the photochemical properties of these compounds.[13]

Theoretical Methods. For the qualitative Hückel π-electron calculation the overlap integrals were as follows: $S_{NN'}$ = 0.19, assuming an orbital exponent[14] of 1.917 and the overlap equations of Mulliken et al.;[15] S_{FeN} = 0.023, assuming an orbital exponent of 3.727 for Fe and the overlap tables of Jaffe.[16] Hückel matrix elements were chosen as follows: $H_{ii}(Fe)$ = −12.70 eV as found in a charge iterative EH calculation[17] for $Fe(CO)_3(C_4H_6)$; $H_{ii}(N)$ = −12.50 eV as determined from best-fit spectroscopic parameters[18] for pyridine and other aromatic nitrogen heterocycles; $H_{FeN} = -2S_{FeN}(H_{ii}(N)H_{ii}(Fe))^{1/2}$, the Ballhausen–Gray approximation[19] to the off-diagonal terms; $H_{NN'} - S_{NN'}E = [S_{NN'}/S_{CC}(C_6H_6)]\beta_0(C_6H_6)$ = −1.95 eV where[18] $\beta_0(C_6H_6)$ = −2.56 eV. All non nearest neighbor interactions were taken to be zero, and the resulting 5 × 5 secular determinant was solved on a TI Programmable 58 calculator with aid of the matrix software. Trial roots required about 4 min of calculator time.

Hartree–Fock–Slater (HFS) calculations[20] of $Fe(CO)_3(N_4H_2)$ were performed on a CDC 6600 computer at the Northwestern University Vogelback Computing Center. The HFS equations were solved iteratively by the discrete variational[21] (DV) procedure and the Coulomb potential approximated by an S-wave potential from the population-charge analysis.[22] An $X\alpha$ exchange parameter of 0.70 was assumed to avoid empiricism. Numerical atomic orbitals from an exact atomic HFS calculation were used as basis functions, and core electrons were included in the calculation with no further approximations. This calculation is of "minimum basis" quality and required about 25 min of CPU time (35 SCF cycles with an 0.17 mixing coefficient) on the 6600 to achieve convergence. For $Fe(CO)_3(N_4H_2)$ the experimental geometry[3] of $Fe(CO)_3(N_4(CH_3)_2)$ was idealized to C_s symmetry (mirror plane bisecting the FeN_4 plane),

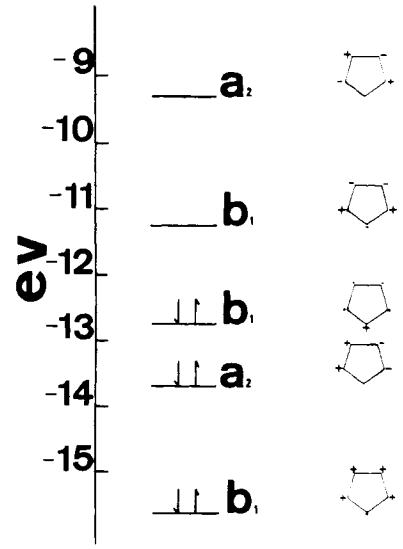

Figure 2. Results from a Hückel π-electron calculation of the FeN_4 ring. Orbital energies and the nodal properties of the 5π orbitals are sketched. The magnitude of the individual atomic contributions are reflected by the size of the orbital ± signs.

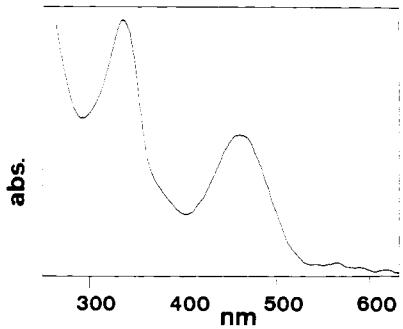

Figure 3. Matrix isolation spectrum of $Fe(CO)_3(N_4(CH_3)_2)$ in argon (greater than 1:1000 dilution) at 10 K. The matrix was deposited onto a sapphire window by the pulsed technique.

and N–H bond lengths of 1.01 Å (H–N–Fe angles of 131°) were assumed. Fractional atomic coordinates are listed in supplementary Table I. A complete tabulation of the ground-state wavefunctions has also been appended as supplementary material. For a test of the sensitivity of our calculations to the N–N bond distances, a second calculation assumed the N_4 ligand geometry found in the related cyclopentadienylcobalt structure.[7] A complete listing of the valence energy levels for this latter calculation have been included as supplementary Table II. These data show the orbital energies and wavefunctions to be relatively insensitive to the change so that no serious qualitative or quantitative errors should result from the bond-length uncertainties. Calculations on the N_4H_2 and $Fe(CO)_3$ fragments employed atomic positions and symmetry orbitals identical with those found in the molecule.

Results and Discussion

Our qualitative analysis of metallocycle π interactions in a $Fe(CO)_3(N_4R_2)$ complex were based on Elain and Hoffmann's[8] theoretical model for the $Fe(CO)_3$ fragment. The highest occupied molecular orbital of this moiety is doubly degenerate, of iron 3d character, and contains two electrons. If bonded to a planar bidentate ligand, the "in-plane" 3d orbital should become σ antibonding, leaving two electrons in an orbital which can overlap with the N_4R_2 ligand in a π sense. From an electron counting point of view, this yields a 6π-electron metallocycle (possibly Hückel aromatic) ring. Results from a Hückel π-electron calculation are provided in Figure 2, along with the π orbital nodal patterns. This agrees with an early[23] Hückel study of the MN_4 moiety. Qualitatively one

(12) A minor modification of the literature[2] procedure.
(13) Johnson, C. E.; Trogler, W. C., manuscript in preparation.
(14) Clementi, E.; Raimondi, D. L. *J. Chem. Phys.* **1963**, *38*, 2686–2689.
(15) Mulliken, R. S.; Rieke, C. A.; Orloff, D.; Orloff, H. *J. Chem. Phys.* **1949**, *17*, 1248–1267.
(16) Jaffe, H. H. *J. Chem. Phys.* **1953**, *21*, 258–263.
(17) Albright, T. A.; Hoffman, P.; Hoffmann, R. *J. Am. Chem. Soc.* **1977**, *99*, 7546–7557.
(18) $H_{ii}(N) = \alpha_0 + \delta\beta_0$, where α_0 was spectroscopically fixed as −10.96 eV (Pariser, R. *J. Chem. Phys.* **1953**, *21*, 568–569; **1956**, *24*, 250–268), β_0 chosen spectroscopically as −2.56 eV (Mulliken, R. S. *J. Chim. Phys.* **1949**, *46*, 675–713), and the δ determined spectroscopically for pyrazine and other nitrogen heterocycles (Lowdin, P. O. *J. Chem. Phys.* **1951**, *19*, 1323–1324). One could argue for other selections of the constants; however, we only use the Hückel results to establish a qualitative origin for discussion.
(19) Ballhausen, C. J.; Gray, H. B. *Inorg. Chem.* **1962**, *1*, 111–122.
(20) Slater, J. C. "The Self-Consistent Field for Molecules and Solids"; McGraw-Hill; New York, 1974.
(21) Ellis, D. E.; Painter, G. H. *Phys. Rev. B* **1970**, *2*, 2887–2898.
(22) Ellis, D. E.; Rosen, A.; Adachi, H.; Averill, F. W. *J. Chem. Phys.* **1976**, *65*, 3629–3634.

Table I. Electronic Absorption Spectral Data (nm) for $FeL_2L'(CH_3N_4CH_3)$ Complexes

L	L'	solvent[a]	λ_{max}^1 (ϵ)	λ_{max}^2 (ϵ)
CO	CO	C_6H_6	467 (2650)	342 (3890)
CO	CO	CH_3OH	467 (2620)	341 (4270)
CO	CO	Ar matrix (10 K)	467	341
CO	$P(OCH_3)_3$	C_6H_6	471 (3060)	349 (3920)
CO	$P(CH_3)_3$	C_6H_6	495 (2550)	360 (3710)
CO	$P(C_6H_5)_3$	C_6H_6	500 (2100)	392 (4250), 368 (3640)
$P(OCH_3)_3$	CO	C_6H_6	461 (2230)	353 (3840)
$P(CH_3)_3$	CO	C_6H_6	482 (2060)[b]	371 (4770)
$P(C_6H_5)_3$	CO	C_6H_6	515 (1600)	388 (7615)
$P(OCH_3)_3$	$P(OCH_3)_3$	C_6H_6	518 (1940)	363 (4340)

[a] All spectra were measured at room temperature unless otherwise noted. [b] A weaker (ϵ_{max} = 510) band was also observed at 602 nm.

finds the HOMO (highest occupied molecular orbital) to be predominantly iron in character and that the LUMO (lowest unoccupied MO), a metallocycle π^* orbital, should lie at optically accessible energies.

Electronic Spectra. Two low-energy electronic transitions signal the presence of the $Fe(N_4R_2)$ chromophore. The 10 K electronic absorption spectrum of $Fe(CO)_3(N_4(CH_3)_2)$ in an argon matrix is displayed in Figure 3. Two intense absorption bands, which are found at 467 and 341 nm, differ by less than ±1 nm from band maxima (Table I) found in various room-temperature solution spectra. It is significant to note the solvent insensitivity of the absorption energies. This result rules out a simple metal to ligand charge-transfer (MLCT) assignment as well as a ligand localized $\eta \rightarrow \pi^*$ transition (i.e., from the lone-pair orbitals on the remote ring nitrogens, N(β), to the π^* orbitals of the tetraazadiene ligand). Simple cis azo compounds exhibit two such transitions $\eta_+ \rightarrow \pi^*$ and $\eta_- \rightarrow \pi^*$, where the + and − signify the two linear combinations of the lone-pair nitrogen orbitals.[24] Although the lowest energy excitation of this type usually occurs between 300 and 400 nm, its intensity would be significantly less than the bands under scrutiny and would be expected to show a strong dependence on solvent polarity.

Effects of chemical substitution prove useful. When the 1,4-dimethyl groups are changed to an aromatic substituent (C_6H_5), the 467- and 341-nm bands *uniformly* red shift by 0.3 eV. Sizeable bathochromic shifts also occur when CO ligands are replaced by more basic ones such as trivalent phosphorus donors (see Table I). An assignment which involves the CO ligands (e.g., Fe → CO π^*) may be ruled out on energetic grounds[25] and by noting the persistence of the absorption bands in the $Fe(P(OCH_3)_3)_3(N_4(CH_3)_2)$ complex. From the experimental evidence, it appears likely that the two low-energy transitions are from upper occupied orbitals with substantial iron d character into the LUMO π^* orbital of the metallocycle moiety. The simple Hückel model of Figure 2 cannot account for these observations, because all of the iron d orbitals were not included. More specific assignments await discussion of a more sophisticated theoretical model.

Photoelectron Spectrum. The gas-phase He I photoelectron spectrum (Figure 4) of $Fe(CO)_3(N_4(CH_3)_2)$ offers many points of interest. There have been several experimental[26] and theoretical[27] studies of the photoelectron spectra of $Fe(CO)_3$(diene) complexes. Orbitals with substantial Fe 3d character are found between 8.1 and 9.2 eV. Unsaturated nitrogen complexes have been extensively studied[28a] and the cis azo moiety

generally exhibits an η_- lone pair IP ca. 8.5 eV, a π ionization

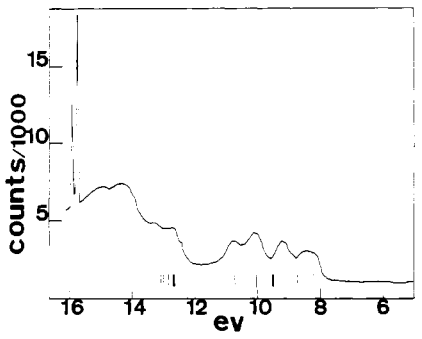

Figure 4. The room-temperature He I photoelectron spectrum of $Fe(CO)_3(N_4(CH_3)_2)$ in the gas phase. Sharp peaks at 15.759 and 15.937 eV are due to argon, which was used as an energy calibrant. The higher occupied molecular orbitals from the Xα calculation are included as vertical lines for comparative purposes.

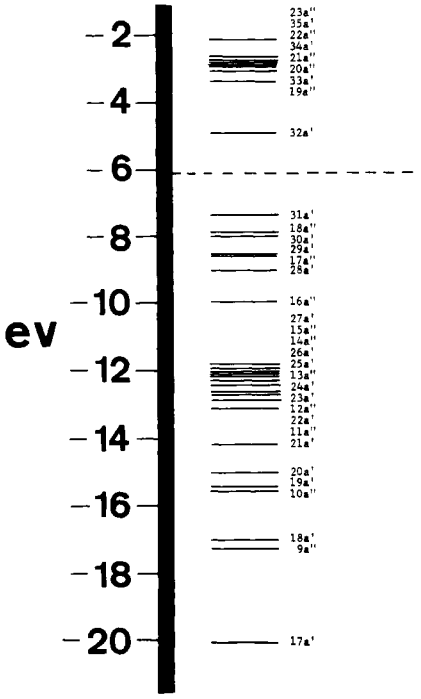

Figure 5. Valence-orbital energy diagram (SCC-DV-Xα) of $Fe(CO)_3(N_4H_2)$. The occupied levels are separated from the unoccupied levels by the dashed line.

(23) Shustorovich, E. M.; Kagan, G. I.; Kagan, G. M. *J. Struct. Chem.* **1970**, *11*, 95–105.
(24) Albini, A.; Kisch, H. *Top. Curr. Chem.* **1976**, *65*, 105–145 and references therein.
(25) Dartiguenave, M.; Dartiguenave, Y.; Gray, H. B. *Bull. Soc. Chim. Fr.* **1969**, *12*, 4223–4225.
(26) Dewar, M. J. S.; Worley, S. D. *J. Chem. Phys.* **1969**, *50*, 654–667. Green, J. C.; Powell, P.; van Tilborg, J. *J. Chem. Soc., Dalton Trans.* **1976**, 1974–1976.
(27) Hall, M. B.; Hillier, I. H.; Connor, J. A.; Guest, M. F.; Lloyd, D. R. *Mol. Phys.* **1975**, *30*, 839–848. Connor, J. A.; Derrick, L. M. R.; Hall, M. B.; Hillier, I. H.; Guest, M. F.; Higginson, B. R.; Lloyd, D. R. *Ibid.* **1974**, *28*, 1193–1205.
(28) (a) Haselbach, E.; Heilbronner, E. *Helv. Chem. Acta* **1970**, *53*, 684–695. Haselbach, E.; Schmelzer, A. *Ibid.* **1972**, *55*, 1745–1752. Houk, K. N.; Chang, Y.; Engel, P. S. *J. Am. Chem. Soc.* **1975**, *97*, 1824–1832. (b) A reviewer pointed out that a metal d_{z^2} orbital can interact strongly with π-accepting basal ligands by mixing in metal p_z character (Rossi, A. R.; Hoffmann, R. *Inorg. Chem.* **1975**, *14*, 365–374). As the metal p_z content of 31 a′ is only 4%, this should not greatly contribute. Furthermore, Figure 9 includes the p contribution.

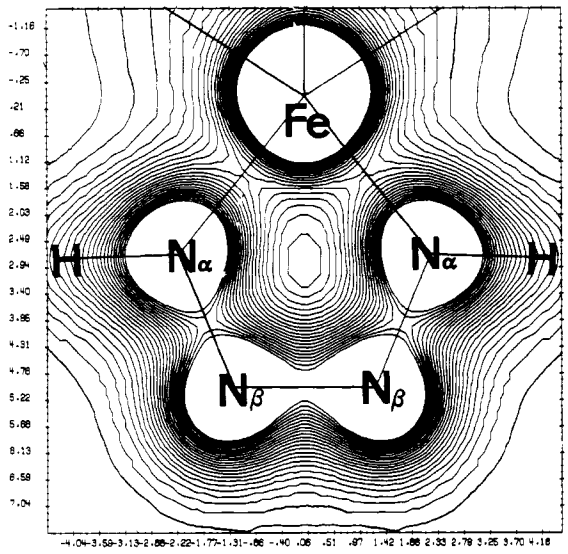

Figure 6. Total electron density in a plane 1 au above the FeN_4H_2 plane. This illustrates the π-electron density distribution. Contour levels are for each 0.0405 e/Å^3 with an upper limit of 1.5 e/Å^3. Therefore, the inner blank areas correspond to regions of high electron density. Small discontinuities are observed because of the finite size of the sampling grid used to compute orbital densities.

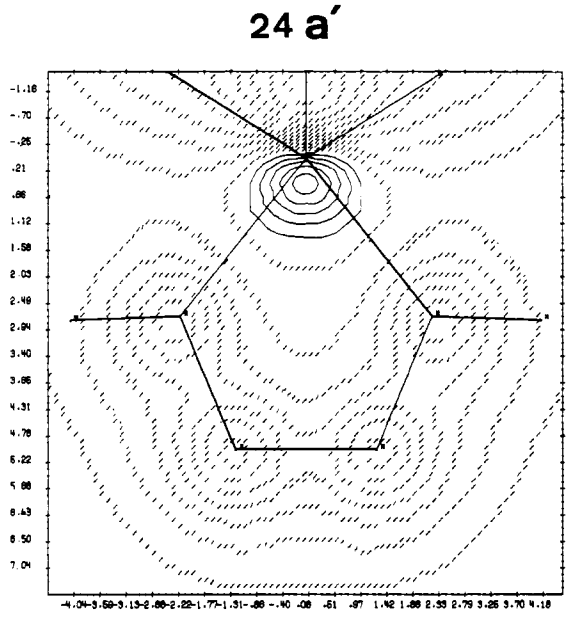

Figure 7. Contour plot for the 24 a′ metallocycle π orbital. Again the plot represents a slice 1 au above the FeN_4H_2 plane; however, the upper cutoff is +1.5 e/Å^3 for the positive contours and −1.0 e/Å^3 for the negative contours.

at approximately 11.0 eV, and the η_+ IP between 11–12 eV. These observations are relevant since ionization from orbitals localized on the CH_3 and CO moieties cannot occur at these low energies. Since an $Fe(CO)_3$ unit possesses 8d electrons and the $N_4(CH_3)_2$ ligand contains 4π electrons and two lone pairs, there are possibly eight orbitals with ionization potentials in the 8.1–12-eV region. Qualitatively this accords with the rich structure exhibited in the low-energy region of the PES.

Theoretical Results. A nonempirical SCC–DV–Xα calculation was performed for the model complex $Fe(CO)_3N_4H_2$. The orbital-energy diagram presented in Figure 5 illustrates the complexity of the problem. Because of the extreme covalency possible in a low-symmetry complex (see Table II), electron density maps are also extremely useful. In Figure 6 the total electron density which lies in a plane 1 au (ca. the

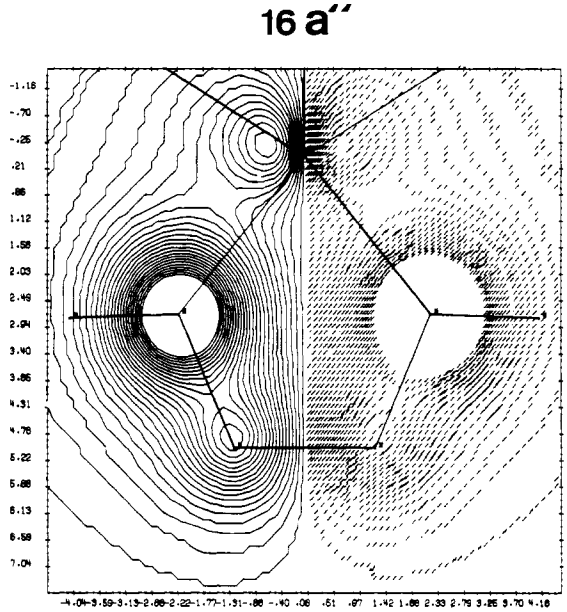

Figure 8. Contour plot for the 16 a″ metallocycle π orbital. Plot parameters are identical with those of Figure 7.

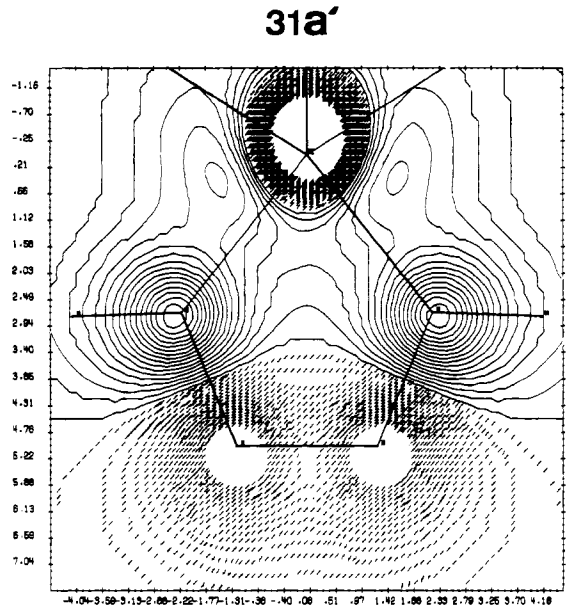

Figure 9. Contour plot for the 31 a′ metallocycle π (HOMO) orbital. Plot parameters are identical with those of Figure 7.

maximum in the radial distribution function for a 2p orbital) above the FeN_4H_2 ring is plotted. This serves to define the coordinates for subsequent plots and illustrates the preferential buildup of π-electron density between the β-nitrogen atoms. Deformation of the charge density about the α-nitrogen atoms from spherical symmetry reflects the N_α–N_β and N_α–Fe π bonding. Qualitative Hückel considerations predicted five metallocycle π orbitals, and 24 a′, 16 a″, 31 a′, 32 a′, and 23 a″ (Figures 7–11) may be so classified. The 6π-electron formulation appears to be correct! Orbitals derived from the Xα procedure do differ significantly from our crude π-electron model. Most striking is the fact that the metal does not employ a single d_π orbital to interact with the N_4H_2 π system. These orbital shapes are determined by the proper linear combination of atomic d functions which minimize the energy of the single particle Hamiltonian employed in the HFS equations. In other words, in low-symmetry systems one must be cautious about too simple orbital models. Note that the 16 a″ metal–ligand

Table II. Valence Orbitals in $Fe(CO)_3(N_4H_2)$ from −30 to −2 eV

		atomic compositions[a] (≥0.05)												
orbital	energy, eV	Fe 3d	N_α 2s	N_α 2p	N_β 2s	N_β 2p	C(1) 2s	C(1) 2p	O(1) 2s	O(1) 2p	C(2) 2s	C(2) 2p	O(2) 2s	O(2) 2p
7a″	−29.41										0.10		0.75	0.07
14a′	−29.39												0.75	0.09
15a′	−28.97						0.11		0.77	0.11				
16a′	−28.35		0.25		0.67	0.06								
8a″	−25.05		0.71		0.17	0.06								
17a′[b]	−21.84		0.47		0.21	0.23								
9a″[c]	−17.43		0.09	0.15	0.23	0.29								
18a′	−17.12						0.08				0.37	0.14	0.10	
10a″	−15.66	0.14									0.43		0.20	0.05
19a′	−15.63	0.07		0.12		0.08	0.32	0.09	0.13					
20a′[d]	−15.25			0.38		0.21	0.08							
21a′	−14.30			0.40		0.17				0.08		0.07		0.12
11a″	−13.24	0.23		0.30							0.07			0.23
22a′	−12.96											0.25	0.15	0.47
12a″	−12.82	0.10		0.15								0.16		0.33
23a′	−12.60							0.09		0.21		0.24		0.26
24a′	−12.52			0.26		0.30					0.07			0.20
13a″	−12.43							0.11		0.12		0.28		0.42
25a′	−12.36	0.10						0.07	0.07	0.20	0.05	0.12		0.22
26a′	−12.27	0.05		0.06		0.08		0.17		0.34		0.05		0.08
14a″	−12.09							0.12		0.19		0.16		0.42
15a″	−11.96							0.12		0.26		0.16		0.40
27a′	−11.92			0.06		0.14		0.16		0.31		0.09		0.13
16a″	−10.01	0.05		0.69		0.12								
28a′	−9.33	0.20		0.13	0.12	0.40								
17a″	−8.79	0.17		0.09	0.21	0.48								
29a′	−8.77	0.73				0.05								0.17
30a′	−8.21	0.46		0.11		0.11				0.10				
18a″	−8.02	0.47		0.16		0.10				0.08				
31a′[e]	−7.51	0.28		0.21		0.15								0.10
32a′	−5.07	0.33		0.21		0.19	0.05							
19a″	−3.63	0.25		0.14		0.06					0.11	0.20		0.11
33a′	−3.43	0.14						0.10		0.06		0.35		0.26
20a″	−3.11	0.15						0.14		0.12		0.28		0.19
21a″	−3.01							0.23		0.19		0.24		0.21
34a′	−2.98	0.09						0.18		0.14		0.29		0.26
22a″	−2.97	0.13						0.05		0.05		0.32		0.21
35a′	−2.94	0.19						0.18		0.14		0.19		0.13
23a″	−2.23			0.24		0.60								

[a] The symbol α denotes the two N atoms bound to Fe and β denotes the remote pair. The C and O atoms which lie in the mirror plane are denoted 1, and those two C and O atoms related by the mirror plane are labeled 2. Fractional atomic contributions were determined as explained in the Experimental Section. [b] H 1s contribution 0.05. [c] H 1s contribution 0.14. [d] H 1s contribution 0.11. [e] Highest occupied molecular orbital.

π-bonding orbital employs a metal δ-type orbital. Orbital 24 a′ has a substantial fraction of metallocycle π character, but it would be misleading to think of it as only metallocycle-localized. Carbon monoxide based atomic functions contribute about equally to 24 a′.

Electron density plots suggest a mechanism for π delocalization. Partial occupation of the lowest π* orbital of the N_4H_2 fragment is evident in the HOMO orbital 31 a′ (Figure 9). A structural consequence of this interaction should be shortening of the N_β–N_β bond and lengthening of the N_α–N_β bonds. As mentioned in the Introduction, there are now a number of examples where these variations have been observed for metal–"tetraazadiene" complexes. Orbital 31 a′ is only weakly antibonding with respect to the Fe–N_α bond since the metal d_{z^2} type orbital overlaps little with the N_α p_π orbital.[28b] Iron participation is therefore relatively nonbonding in this instance.

Essential features of the Fe–N_4H_2 interaction are defined by a fragment analysis. Results of SCC–DV–Xα computations for the $Fe(CO)_3$ and N_4H_2 fragments are summarized in Tables III and IV. Of considerable importance is the fact that the LUMO 9 a′ (π*) orbital of the N_4H_2 fragment lies below the HOMO 23 a′ level of the $Fe(CO)_3$ moiety. Consequently, one expects charge flow from the metal to ligand fragment. This interaction yields the 31 a′ and 32 a′ MO's of Figures 9 and 10.

Table III. Valence Orbitals in N_4H_2[a]

orbital	energy, eV	N_α 2s	N_α 2p	N_β 2s	N_β 2p	H
3a′	−27.22	0.22		0.70		0.01
3a″	−24.05	0.62		0.21	0.05	
4a′	−20.56	0.42	0.06	0.16	0.25	
4a″	−15.78	0.11	0.43	0.25		0.17
5a′	−14.38		0.41		0.36	0.19
6a′	−11.75	0.12	0.31	0.10	0.46	
7a′ (π)	−11.22		0.21		0.79	
5a″	−9.60	0.05	0.30	0.20	0.37	0.08
6a″ (π)	−8.19		0.75		0.25	
8a′	−6.99	0.12	0.43	0.06	0.34	0.04
7a″[b]	−6.22		0.51	0.19	0.17	0.03
9a′ (π*)	−5.12		0.67		0.33	
8a″ (π*)	−1.43		0.34		0.66	

[a] Symbols α and β refer to the convention specified in Table II. [b] Denotes highest occupied orbital.

Atomic charge densities also mirror this effect. Data in Tables V and VI show that the N_α atoms accept considerable π charge density from the iron tricarbonyl moiety upon complex formation. This result sharply contrasts with an earlier CNDO study[29] of $Fe(CO)_3(N_4H_2)$ which showed a buildup

(29) Armstrong, D. R.; Perkins, P. G.; Scott, J. M.; Stewart, J. J. P. *Theoret. Chim. Acta (Berlin)* **1972**, *26*, 237–248.

Table IV. Valence Orbitals in $Fe(CO)_3$

		atomic compositions[a] (≥0.05)								
orbital	energy, eV	Fe 3d	C(1) 2s	C(1) 2p	O(1) 2s	O(1) 2p	C(2) 2s	C(2) 2p	O(2) 2s	O(2) 2p
14a′	−16.42		0.11	0.05			0.43	0.20	0.13	
6a″	−15.34	0.05					0.47	0.12	0.22	0.07
15a′	−15.04		0.37	0.09	0.16		0.11		0.05	
16a′	−12.84							0.20	0.16	0.52
7a″	−12.72	0.10					0.05	0.18	0.15	0.49
17a′	−12.38	0.09		0.15	0.15	0.43				
18a′	−12.27			0.39		0.05				0.45
8a″	−12.08							0.35		0.54
19a′	−12.06	0.05						0.39		0.47
9a″	−11.77			0.09		0.12		0.26		0.50
20a′	−11.64			0.30		0.56				
10a″	−11.46			0.22		0.44		0.10		0.23
11a″	−7.95	0.79				0.09				
21a′	−7.92	0.73								0.20
22a′	−7.59	0.76				0.09				0.09
23a′[b]	−6.21	0.55	0.06							
12a″[c]	−6.15	0.57					0.11			0.07

[a] Column headings follow the convention of Table II. [b] Highest occupied orbital and contains 0.14 Fe 4p character. [c] This orbital also contains 0.14 Fe 4p character.

Table V. Gross Atomic Charges and Valence Occupation Numbers in $Fe(CO)_3(N_4H_2)$

atom	charge	valence occupation nos.
Fe[a]	+1.09	d (6.98)
N_α	−0.43	s (1.58), p (3.84)
N_β	−0.04	s (1.56), p (3.48)
H	+0.29	s (0.71)
C(1)	−0.10	s (1.41), p (2.69)
C(2)	−0.12	s (1.42), p (2.70)
O(1)	−0.15	s (1.87), p (4.27)
O(2)	−0.13	s (1.83), p (4.29)

[a] Valence s and p contributions ≤1% for Fe. The symbol α denotes the two N atoms bound to Fe and β denotes the remote pair. The C and O atoms which lie in the mirror plane are denoted 1, and those two C and O atoms related by the mirror plane are labeled 2.

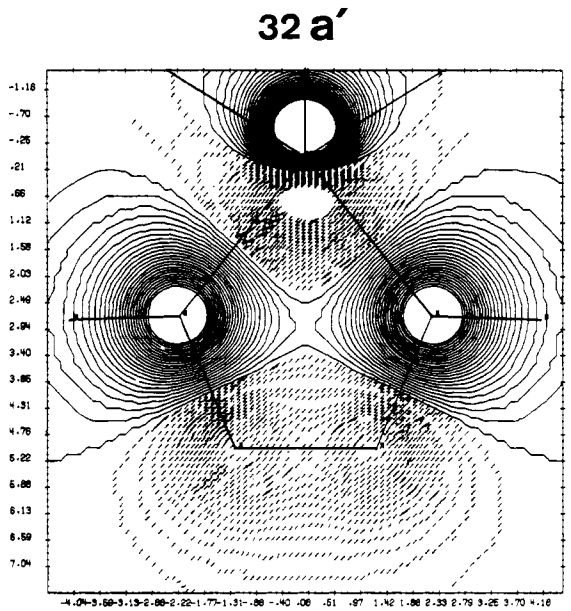

Figure 10. Contour plot for the 32 a′ metallocycle π^* (LUMO) orbital. Plot parameters are identical with those of Figure 7.

of electron density on iron and a decrease of π-electron density on the N_4H_2 ligand. Some experimental evidence can be cited which supports our model. Stretching frequencies of carbon monoxide frequently reflect the available π-electron charge density at the metal in homologous complexes.[30] We have

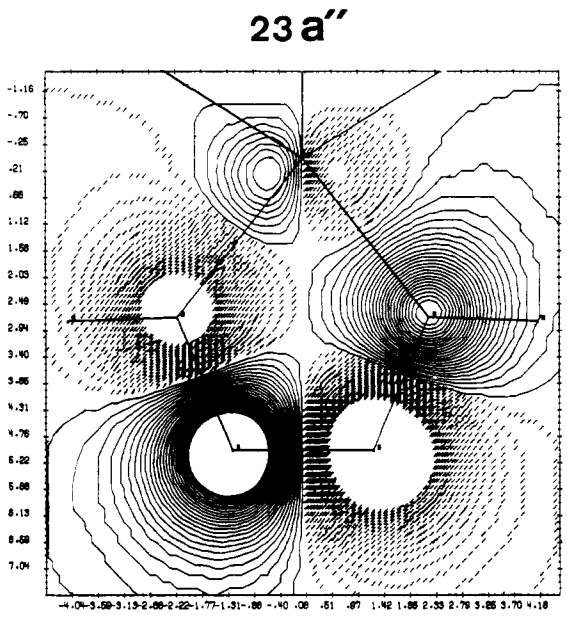

Figure 11. Contour plot for the 23 a″ metallocycle π^* orbital. Plot parameters are identical with those of Figure 7.

Table VI. Gross Atomic Charges and Valence Occupation Numbers in the N_4H_2 and $Fe(CO)_3$ Fragments

atom[a]	charge	valence occupation nos.
N_α	−0.31	s (1.68), p (3.62)
N_β	−0.04	s (1.57), p (3.47)
H	+0.35	s (0.65)
Fe	+0.81	d (7.06)
C(1)	−0.15	s (1.47), p (2.68)
C(2)	−0.12	s (1.37), p (2.75)
O(1)	−0.14	s (1.82), p (4.31)
O(2)	−0.14	s (1.82), p (4.32)

[a] Abbreviations used are the same as in Table V.

measured the infrared spectrum of $Fe(CO)_3(N_4(CH_3)_2)$ in the gas phase. A band at 2072.06 cm^{-1} exhibits resolved P, Q, and R branches while the fine structure is not resolved for a more intense band at 2006.76 cm^{-1}. With Braterman's criteria,[31] these are the a_1 and e CO stretching modes of the

(30) Tolman, C. A. *J. Am. Chem. Soc.* **1970**, *92*, 2953–2956. Jolly, W. L.; Avanzino, S. C.; Rietz, R. R. *Inorg. Chem.* **1977**, *16*, 964–966.

$Fe(CO)_3$ moiety. The degeneracy weighted average of 2028.5 cm^{-1} is identical with that (2028.6 cm^{-1}) computed from the vibrational data reported[32] for $Fe(CO)_5$. This constitutes prima facie evidence that the π-acceptor ability of $N_4(CH_3)_2$ is comparable to that of two carbon monoxides, a remarkable fact, since few other ligands approach CO in their π-acceptor ability.

Only one other atom markedly alters its charge upon molecule formation and that is hydrogen. It is reasonable that, as N_α accepts electron density from the metal, the demand on the α substituent should be less. The observation also points out that electron-withdrawing substituents should increase the π-acceptor properties of the N_4R_2 ligand. An extreme case, documented by accurate crystallographic results and supported by Xα calculations,[7] is the complex $Co(\eta^5\text{-}C_5H_5)(N_4R_2)$ where $R = C_6F_5$.

The nature of the 32 a′ orbital resembles 31 a′ except for the nature of the d_π–N_α p_π interaction, which is somewhat more antibonding than in 31 a′. From Figure 5 it is evident that this unoccupied orbital lies well below all other virtuals. Therefore, low-lying one-electron transitions in the tetraazadiene complexes[5] would be expected to terminate in this orbital. Spin-restricted transition-state calculations[33] place the 31 a′ → 32 a′, 18 a″ → 32 a′, and 30 a′ → 32 a′ electronic transitions at 2.48, 3.00, and 3.2 eV. Considering the limited description of virtual orbital space, these values agree reasonably well with the intense absorptions at 2.66 and 3.63 eV in the electronic absorption spectrum of $Fe(CO)_3(N_4(CH_3)_2)$. Calculations then suggest a near degeneracy of the second electronic absorption band. Orbitals 18 a″ and 30 a′ derive from an e orbital[8] of the $Fe(CO)_3$ fragment. Negligible splitting of the e CO stretching mode (vide supra) in $Fe(CO)_3(N_4(CH_3)_2)$ provides experimental evidence that the $Fe(CO)_3$ fragment maintains pseudo C_{3v} symmetry in the molecule. The lowest allowed electronic transition to a CO-based π^* level (31 a′ → 19 a″) is calculated to occur at 3.91 eV (317 nm) and cannot be responsible for the low-energy absorptions.

In-plane and out of plane (by 1 au) contour plots for other FeN_4 localized molecular orbitals will now be summarized. In plane Fe d–N_α σ bonding dominates the composition of 21 a′ which also exhibits significant N_β–N_β σ-bond character. The negative lobes of both these σ bonds are oriented so that in plane π overlap takes place between them. The N_β–N_β σ bond is concentrated in the 28 a′ orbital, and the negative tail of the bonding orbital on each N_β atom contributes density to the N_β lone-pair region. Some overlap with the N_α–H σ bond also occurs. The 29 a′ orbital is primarily an in plane cloverleaf iron d orbital ($d_{x^2-y^2}$) with one lobe directed between the N_α atoms. As a result there is only a weak-bonding interaction with the N_4H_2 ligand. This contrasts with the complex iron d character of 30 a′ which points between the N_α atoms, π bonds with terminal carbon monoxide ligands, and is σ antibonding with respect to the N_α atoms. Some N_β–N_β σ-bond character also persists in this orbital.

Strong σ bonding occurs between an in-plane cloverleaf iron d orbital (d_{xy}) which points at the N_α atoms and N_α sp hybrids in the 11 a″ level. This orbital, however, is dominated by N_α–N_β σ bonding and some N_β lone-pair character. Orbital 17 a″ predominantly consists of N_β lone-pair contributions. The 18 a″ orbital is rather diffuse, containing appreciable iron d_σ and d_{π^*} character with respect to N_α (a reviewer suggested describing this as an antibonding counterpart of 16 a″). In addition, some N_β lone pair–N_α σ character and Fe–CO π-bonding character are evident. Atomic compositions of other orbitals are summarized in Table II, and complete wavefunctions are available as supplementary material.

In Figure 4 we have compared the calculated relative orbital energies of $Fe(CO)_3(N_4H_2)$ with the low-energy features in the photoelectron spectrum of $Fe(CO)_3(N_4(CH_3)_2)$. Although some caution[34] is necessary with such comparisons, it is encouraging that the calculated width of the low-energy band of ionizations appears correct. Perhaps more significant, the gap between the low-energy and high-energy features looks about right. Ionizations in the 8–11-eV region are therefore assigned to the 31 a′–16 a″ orbitals of Table II. Note this total is one short of our earlier qualitative prediction of eight low-energy IP's. Orbitals 31 a′–29 a′ are (approximately) the four IP's associated with the d^8 metal complex as can be seen from the atomic compositions in Table II; however, 31 a′ contains much N_4H_2 π^* character. The two N_β lone-pair orbitals are roughly 17 a″ and 28 a′. The difference between the quantitative and qualitative predictions derives from the presence of only one N_4H_2 π ionization, 16 a″, in the low-energy region. Extensive π delocalization imparts special stability to 24 a′ (Figure 7) and explains the discrepancy.

Conclusion. Iron tricarbonyl tetraazadiene complexes contain an FeN_4 moiety which exhibits extreme delocalization that is characteristic of a 6π electron metallo aromatic ring. In π acceptor–π donor terminology, the 9 a′ (π^*) level of the tetraazadiene accepts electron density from occupied d_π and d_δ orbitals on the $Fe(CO)_3$ fragment. The unusually low energy of the N_4R_2 π^* orbital apparently accounts for the fact that metallotetraazadiene complexes exhibit π delocalization, while metallocyclopentadiene complexes do not. Calculations for the latter systems[1] place the empty C_4R_4 π^* orbital at energies well above the occupied metal d_π orbitals. Quantitative Xα calculations provide reasonable assignments of the electronic absorption spectrum and He(I) photoelectron spectrum of $Fe(CO)_3(N_4(CH_3)_2)$. The presence of a low-lying unoccupied metallocycle π^* orbital (32 a′) explains the two intense low-energy features which characterize electronic absorption spectra of compounds which contain the $Fe(N_4R_2)$ moiety.

Acknowledgment is made to the donors of the Petroleum Research Fund, administered by the American Chemical Society, for partial support of this research. Continued support by the National Science Foundation (Grant CHE78-01615) is gratefully acknowledged, and we thank Northwestern University's Vogelback Computing Center for a grant of machine time. W.C.T. appreciates support by the Rohm and Haas Co. in the form of a summer (1980) faculty fellowship. We thank Professor Robert Doedens for communicating some unpublished structural results, Dr. J. Berkowitz and the Physics Division of Argonne National Laboratories for access to their photoelectron spectrometer, and Professors Roald Hoffmann and Michael Hall for insightful comments.

Registry No. $Fe(CO)_3(N_4(CH_3)_2)$, 38668-89-2; $Fe(CO)_2(P(OCH_3)_3)(N_4(CH_3)_2)$, 76299-41-7; $Fe(CO)_2(P(CH_3)_3)(N_4(CH_3)_2)$, 76299-42-8; $Fe(CO)_2(P(C_6H_5)_3)(N_4(CH_3)_2)$, 76299-43-9; $Fe(CO)(P(OCH_3)_3)_2(N_4(CH_3)_2)$, 76299-44-0; $Fe(CO)(P(CH_3)_3)_2(N_4(CH_3)_2)$, 76299-45-1; $Fe(CO)(P(C_6H_5)_3)_2(N_4(CH_3)_2)$, 76299-46-2; $Fe(P(OCH_3)_3)_3(N_4(CH_3)_2)$, 76299-47-3; $Fe(CO)_3(N_4H_2)$, 76299-48-4; $Fe(CO)_3(N_4(C_6H_5)_2)$, 76299-49-5.

Supplementary Material Available: Tables of the ground-state wavefunctions and atomic positions for $Fe(CO)_3(N_4H_2)$ and orbital energies of $Fe(CO)_3(N_4R_2)$ for a different choice of N–N bond lengths in tabular form (11 pages). Ordering information is given on any current masthead page.

(31) Braterman, P. S. "Metal Carbonyl Spectra"; Academic Press: New York, 1975; pp 144–146.
(32) For a report on a_1', a_1', a_2'' and e′ C–O stretching features at 2116, 2030, 2019, and 1989 cm^{-1}, see: Jones, L. H.; McDowell, R. S.; Goldblatt, M.; Swanson, B. I. *J. Chem. Phys.* **1972**, *57*, 2050–2064.
(33) See ref 20 and 22 for details.
(34) Heilbronner, E.; Schmelzer, A. *Nouv. J. Chim.* **1980**, *4*, 23–28.